Helpa, V., Rybacki, E., Abart, R., Morales, L. F. G., Rhede, D., Jeřábek, P., Dresen, G. (2014): Reaction kinetics of dolomite rim growth. - *Contributions to Mineralogy and Petrology*, *167*

DOI: http://doi.org/10.1007/s00410-014-1001-y

Reaction kinetics of dolomite rim growth

V. HELPA[1*], E. RYBACKI[1], R. ABART[2], L.F.G. MORALES[1], D. RHEDE[1], P. JEŘÁBEK[3], G. DRESEN[1]

[1]GFZ Potsdam, Telegrafenberg, 14473 Potsdam, Germany
(*correspondence: vanessa.helpa@gfz-potsdam.de)
[2] University of Vienna, Althanstrasse, 1090 Wien, Austria
[3] Charles University, Albertov 6, 12843 Prague, Czech Republic

Abstract

Reaction rims of dolomite ($CaMg[CO_3]_2$) were produced by solid-state reactions at the contacts of oriented calcite ($CaCO_3$) and magnesite ($MgCO_3$) single crystals at 400 MPa pressure, 750-850 °C temperature and 3-146 h annealing time to determine the reaction kinetics. The dolomite reaction rims show two different microstructural domains. Elongated palisades of dolomite grew perpendicular into the magnesite interface with length ranging from about 6 μm to 41 μm. At the same time, a 5-71 μm wide rim of equiaxed granular dolomite grew at the contact with calcite. Platinum markers showed that the original interface is located at the boundary between the granular and palisade-forming dolomite. In addition to dolomite, a 12 to 80 μm thick magnesio-calcite layer formed between the dolomite reaction rims and the calcite single crystals. All reaction products show at least an axiotactic crystallographic relationship with respect to calcite reactant, while full topotaxy to calcite prevails within the granular dolomite and magnesio-calcite. Dolomite grains frequently exhibit growth twins characterized by a rotation of 180° around one of the $[11\bar{2}0]$ equivalent axis. From mass balance considerations it is inferred that the reaction rim of dolomite grew by counter diffusion of MgO and CaO. Assuming an Arrhenius type temperature dependence, activation energies for diffusion of CaO and MgO are E_a (CaO) = 192 ± 54 kJ/mol and E_a (MgO) = 198 ± 44 kJ/mol, respectively.

Introduction

Mineral reactions in the solid-state are ubiquitous in the Earth's crust and mantle. Unless deformed or overprinted, the product phases of such solid-state reactions are commonly located along former phase boundaries between reactants, forming polycrystalline or polyphase reaction rims or coronas (ASHWORTH ET AL. 1998; KELLER ET AL. 2006; KELLER, WIRTH, ET AL. 2008; KELLER, WUNDER, ET AL. 2008). They may contain information about the pressure, temperature and time conditions of their formation and therefore provide a useful indication on the geological history (KELLER, WIRTH, ET AL. 2008; JOACHIM ET AL. 2010).

For a solid-state reaction under "dry" conditions, the necessary transfer of matter between the reactants occurs by diffusion leading to reaction rim growth with kinetics that depends on P-T-t conditions (LASAGA 1983). To constrain the diffusion kinetics using microstructure analysis, knowledge of the component mobility and the transport mechanisms are required. In a polyphase aggregate, the transfer of chemical components may occur via a

combination of grain boundary- and volume diffusion, with grain boundary (GB) diffusion typically being several orders of magnitude faster than diffusion through the volume of the grains. GB diffusion thus is effective over larger spatial scales (DOHMEN AND MILKE 2010). However, at elevated temperatures the contribution of volume diffusion to the bulk mass transfer may increase considerably owing to higher activation energy than for grain boundary diffusion (MROWEC 1980). In general, the growth behaviour of solid-solid reaction rims can be described by the relation: $\Delta x^n = kt$, where Δx is the thickness of the reaction layer, k is a rate constant, t is time and n is a parameter depending on the reaction controlling mechanism (SCHMALZRIED 1978; KELLER ET AL. 2010). For interface-reaction controlled growth n = 1 and for diffusion controlled growth n = 2. It has been demonstrated by ABART AND PETRISHCHEVA (2011) that, after an incipient nucleation phase, reaction rim growth is initially interface reaction-controlled, replaced by diffusion-controlled growth as the rim thickness increases. From the rate of reaction rim growth in the diffusion controlled kinetic regime the mobility of the respective components can be inferred. This motivated a series of rim growth experiments that aimed to determine component mobility. Dedicated studies exist for several systems such as $CaCO_3$-SiO_2, where wollastonite is formed between calcite and quartz (MILKE AND HEINRICH 2002), MgO-SiO_2, where enstatite is formed between forsterite and quartz, or enstatite-forsterite double layers are formed between periclase and quartz (e.g. GARDÉS & HEINRICH, 2011; GÖTZE ET AL., 2009; MILKE, WIEDENBECK, & HEINRICH, 2001), and MgO-Al_2O_3 where spinel is formed between periclase and corundum (e.g. GÖTZE ET AL., 2009; KELLER ET AL., 2010; WATSON & PRICE, 2002). For grain boundary diffusion-controlled growth, the reaction kinetics may be influenced by grain size (GARDÉS ET AL. 2011; GARDÉS AND HEINRICH 2011), water content (GARDÉS ET AL. 2012; MILKE ET AL. 2009; MILKE ET AL. 2012), and non-hydrostatic stress (GÖTZE ET AL. 2009; KELLER ET AL. 2010). In contrast, little is known about diffusion-controlled reactions in the system $CaCO_3$-$MgCO_3$, i.e. the formation of dolomite [$(CaMg(CO_3)_2$] between calcite ($CaCO_3$) and magnesite ($MgCO_3$). So far, few cation diffusion data are available for diffusion in dolomite. ANDERSON (1972) determined self-diffusion of C and O in dolomite at T = 645 to 785°C and P = 12 to 93.5 MPa and MÜLLER, CHERNIAK, & WATSON (2012) investigated cation exchange between dolomite and siderite or rhodochrosite to determine volume diffusion of (Mn, Fe) – Mg – Ca at T = 400-625°C, P = 0.1 MPa.

In this study reaction rims of dolomite were produced at contacts between oriented natural calcite and magnesite single crystals following the reaction:

$$MgCO_{3,solid} + CaCO_{3,solid} = CaMg(CO_3)_{2,solid} \quad \textbf{(1)}$$

The experiments were performed at T = 750-850°C and P_c = 400 MPa to determine the reaction kinetics of dolomite rim growth in the carbonate system under static annealing conditions.

Experimental and analytical details

Starting material

The starting materials were prepared from natural calcite single crystals from Mina Prieta Linda, Naica (Chihuahua, Mexico) and Minais Gerais (Brasil) and from magnesite single crystals from Bahia (Brumado, Brasil). The chemical composition was analyzed by field emission gun electron microprobe (JEOL JXA-8500 F HYPERPROBE), using 15 keV accelerating voltage, 5 nA beam current and 1 μm beam diameter. The results are given in **Table 1**, revealing trace amounts of Fe and Mg in calcite. Magnesite contained impurities of Ca, Fe and traces of Mn, Ba, and Sr. The water content estimated from Vario EL III element analyser (Elementar Analysesysteme GmbH) is about 0.15 wt.% and 0.25 wt.% in calcite and magnesite, respectively.

	Calcite ± 1σ	Magnesite ± 1σ
MgO	0.03 ± 0.04	46.08 ± 1.65
FeO	0.04 ± 0.05	0.18 ± 0.05
CaO	53.37 ± 0.76	0.26 ± 0.04
SrO	0.02 ± 0.03	0.02 ± 0.01
MnO	0.01 ± 0.03	0.04 ± 0.03
TiO_2	0.01 ± 0.02	0.01 ± 0.01
SiO_2	0.00 ± 0.01	0.01 ± 0.02
BaO	0.00 ± 0.01	0.04 ± 0.03
CO_2	46.51± 0.74	53.36 ± 1.66

Table 1 Composition of starting materials in wt.%. Values represent mean data based on 5 point analyses. CO2 contents were calculated assuming an oxide total of 100%

Annealing experiments

Cylindrical samples of 3-5 mm length and 7 mm diameter were drilled out of the single crystals, oriented with the cylinder axis perpendicular to the cleavage planes of the rhombohedra $[(10\bar{1}4), (\bar{1}104), (0\bar{1}14)]$. Subsequently samples were polished with diamond powder to a surface roughness of 1 μm. In three experiments (CaMg-13, CaMg-14, CaMg-15, **Table 2**), both contact surfaces of calcite and magnesite were polished to 0.25 μm finish and sputtered with a thin platinum layer (< 2nm), which served as a marker to locate the initial calcite-magnesite interface after formation of the rims. The assembly for each run consisted of a calcite-magnesite sandwich, located between alumina spacers and adjacent alumina pistons **Figure 1**.

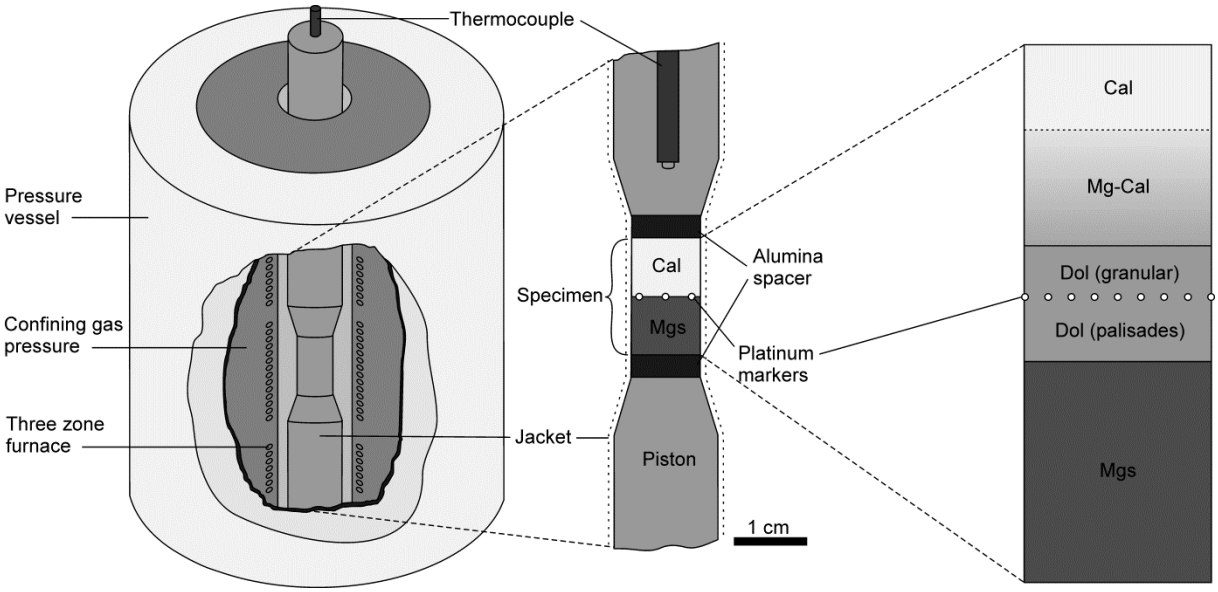

Figure 1 Experimental setup. The sample assembly consists of polished cylinders of calcite and magnesite single crystals. The dolomite reaction rim grows from the initial calcite-magnesite contact into both directions. The initial calcite-magnesite contact is marked by platinum markers (white dots) in some experiments. Adjacent magnesio-calcite evolved next to calcite reactant

The whole assembly was jacketed by a copper-sleeve to prevent intrusion of the confining pressure medium (argon-gas). Temperature was measured using a Pt/Pt-13%Rh (R-type) thermocouple 3 mm from the sample assembly. All experiments were performed in an internally heated pressure vessel using a Paterson type gas deformation apparatus (PATERSON 1970) at a confining pressure of P_c = 400 MPa. Temperatures were kept constant at 750°C, 800°C, 825°C or 850°C with a heating rate of 20°C/min and a cooling rate of 2°C/min (**Table 2**). After the experiments, the jacketed sample assembly was cut along the cylinder axis using a slow-speed diamond saw, embedded in epoxy and the surfaces were polished down to 1 μm roughness for analysis of the reaction rim.

Experiment	T (K)	t (h)	Δx_{Dol} (µm)	Δx_{Pal} (µm)	Δx_{gran} (µm)	$\Delta x_{Mg\text{-}Cal}$ (µm)	a_{Pal} (µm)	a_{gran} (µm)	$a_{Mg\text{-}Cal}$ (µm)	Log D_{CaO} (m^2/s)	Log D_{MgO} (m^2/s)
CaMg-02	1073	74.03	36.3 ± 5.3	16.5 ± 3.1	20.2 ± 4.3	55.0 ± 10.7	3.6 ± 0.9	5.4 ± 1.9	39.0 ± 20.1	-14.4 ± 0.3	-14.2 ± 0.3
CaMg-03	1023	73.95	14.9 ± 5.3	10.5 ± 4.0	7.5 ± 3.0	40.9 ± 10.4	3.1 ± 1.1	2.7 ± 1.1	23.3 ± 12.9	-14.6 ± 0.4	-14.6 ± 0.4
CaMg-04	1023	50.07	17.5 ± 5.7	9.0 ± 2.8	8.3 ± 3.1	27.3 ± 8.3	2.9 ± 0.9	3.2 ± 1.3	22.2 ± 16.0	-14.6 ± 0.5	-14.5 ± 0.5
CaMg-05	1023	145.77	26.0 ± 6.0	12.3 ± 3.0	13.8 ± 4.4	37.2 ± 6.1	3.9 ± 1.0	4.0 ± 1.3	37.3 ± 17.3	-14.8 ± 0.4	-14.7 ± 0.4
CaMg-06	1073	144.71	40.9 ± 7.1	16.2 ± 4.2	24.5 ± 4.9	74.2 ± 11.6	4.3 ± 1.4	4.2 ± 1.4	44.3 ± 23.9	-14.7 ± 0.3	-14.4 ± 0.3
CaMg-07	1073	84.82	30.0 ± 7.2	14.7 ± 3.3	17.1 ± 5.1	37.0 ± 7.3	4.1 ± 1.2	4.6 ± 1.4	35.7 ± 15.4	-14.4 ± 0.4	-14.3 ± 0.4
CaMg-08	1073	48.1	25.4 ± 7.1	12.1 ± 3.4	14.8 ± 4.2	48.5 ± 8.2	3.3 ± 0.8	3.9 ± 1.2	38.2 ± 23.4	-14.4 ± 0.5	-14.2 ± 0.5
CaMg-09	1023	2.44	2.9 ± 1.2	NA	NA	12.1 ± 4.2	NA	NA	12.7 ± 4.7	NA	NA
CaMg-10	1123	74.15	103.7 ± 33.5	41.3 ± 10.2	71.0 ± 18.2	80.3 ± 21.2	5.0 ± 1.2	4.3 ± 1.3	45.8 ± 32.9	-13.4 ± 0.7	-13.4 ± 0.7
CaMg-12	1073	4.03	11.3 ± 4.2	6.0 ± 2.4	5.4 ± 2.4	20.0 ± 5.5	1.7 ± 0.4	2.6 ± 0.9	18.5 ± 9.7	-13.9 ± 0.6	-13.8 ± 0.6
CaMg-13*	1098	74.92	40.1 ± 9.5	17.3 ± 5.1	17.0 ± 5.0	52.3 ± 13.3	4.3 ± 1.1	1.4 ± 0.8	42.0 ± 27.7	-14.2 ± 0.5	-14.2 ± 0.5
CaMg-14*	1073	28.94	14.2 ± 4.9	8.3 ± 3.1	5.8 ± 2.5	31.2 ± 8.3	2.4 ± 0.8	2.9 ± 1.2	26.1 ± 15.4	-14.4 ± 0.5	-14.4 ± 0.5
CaMg-15*	1023	29.13	13.0 ± 1.6	6.8 ± 2.4	5.0 ± 2.8	31.5 ± 10.2	2.6 ± 0.6	2.5 ± 0.8	26.6 ± 14.0	-14.6 ± 0.2	-14.6 ± 0.2

*Platinum marker experiment

Table 2 Average thickness of entire dolomite (Δx_{Dol}), dolomite palisades (Δx_{Pal}), granular dolomite layers (Δx_{gran}), and magnesio-calcite ($\Delta x_{Mg\text{-}Cal}$). a_{Pal}, a_{gran} and $a_{Mg\text{-}Cal}$ are the mean grain diameter of dolomite palisades, granular dolomite and magnesio-calcite, respectively. D_{CaO} and D_{MgO} are the derived diffusion coefficients of CaO and MgO. Uncertainties are given as 1σ value

The run conditions and the results of 13 annealing experiments are presented in **Table 2**. Dolomite reaction rims were produced during static annealing tests of 13 samples with annealing times between 3 and 146 hours (**Table 2**).

Figure 2 shows the polybaric (200-850 MPa) phase diagram for $CaCO_3$-$MgCO_3$ adopted from GOLDSMITH AND HEARD (1961), revealing that both dolomite and magnesio-calcite are stable at the applied experimental conditions. Compared to the solvi shown in

Figure 2, the experimental pressure of 400 MPa slightly increases the solubility of $MgCO_3$ in calcite by about 1 mol % at 750°C and 2% mol % at 850°C, respectively (GOTTSCHALK AND METZ 1992).

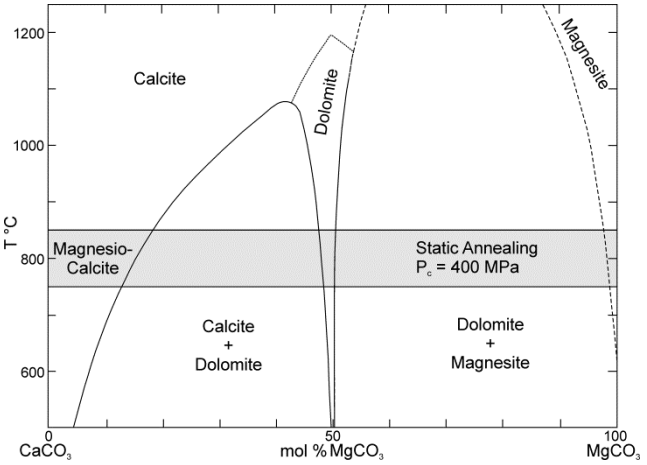

Figure 2 Phase relations of calcite, dolomite and magnesite in the Ca-Mg carbonate system (modified after GOLDSMITH AND HEARD 1961). The experimental temperature range for static annealing tests is indicated by the grey box

Analytical methods

For determination of the dolomite and magnesio-calcite reaction layer thicknesses we used an optical microscope (Leica DM RX) to obtain a complete set of reflected-light micrographs across the whole sample diameter. The width of reaction rims was subsequently analyzed by digitizing the location of phase boundaries and calculation of average values owing to the relatively large thickness variation up to 41 % along a single profile. The associated run durations were corrected for additional growth during heating and cooling ramps (Lasaga 1983), but the effect is negligible.

Microprobe analysis of the composition profiles across selected reaction rims was performed by quantitative line scans using wavelength dispersive X-ray (WDS) measurements, counting only the major elements Ca (Kα, PETJ) and Mg (Kα, TAP). For the analysis, we applied an accelerating voltage of 15 kV and a beam current of 5 nA. Counting time was 5 s on the peak, step size 2 μm and the beam diameter was 1 μm.

The crystallographic orientations of the reactant and product phases were measured using a dual-beam scanning electron microscope (FEI Quanta 3d FEG SEM-FIB), equipped with an electron backscatter diffraction detector (EBSD, TSL DigiView) and a semi-quantitative energy dispersive spectroscopy (EDS) mapping device. Since calcite, dolomite and magnesite have very close unit cell parameter a, b, c the EBSD patterns of these three phases are very similar. Therefore, we used EBSD and EDS mapping to discriminate the three minerals by measuring the

Mg and Ca content. First, we mapped the reactants and the reaction rim using only the calcite reflector list, together with EDS analysis. Subsequently, we identified the three-phases based on the Mg/Ca ratios (e.g., Mg-rich – magnesite; Mg/Ca – dolomite; Ca-rich – calcite). Finally, the inspected area was remapped using the reflectors of all three phases. The magnesio-calcite was discriminated separately using microprobe analysis. For EBSD analysis, the samples were first mechanically polished to 0.25 μm roughness using a diamond paste and afterwards chemically-mechanically polished for one hour using an alkaline solution of colloidal silica. To avoid carbon coating, measurements were conducted in low-vacuum with a chamber pressure of 10 Pa of H_2O. Automatic mappings of selected areas were performed using an accelerating voltage of 15 keV, a step size between 0.5 and 2 μm, a working distance of 15 mm and a beam current of 8 nA. The TSL-OIM software (ADAMS, WRIGHT, AND KUNZE 1993) was used to index and analyze the EBSD patterns. Post-acquisition treatment of the raw EBSD data included the standardization of the confidence index (CI) and the CI correlation between neighbour points, assuming a value of 0.2. After processing, the points with CI < 0.2 were removed from the datasets to avoid incorrect measurements. In general, the CI ranges from 0 to 1 and quantifies the relationship between the number of votes that each phase receives during the indexation of patterns in EBSD mapping. A CI value of 0.2 indicates that the patterns are correctly indexed by about ~99 %. Pole figures were plotted as one point per grain in a reference frame where the E-W plane is parallel to the reaction interface, and the pole of this plane indicates the growing direction (GD) of the reaction rim.

Results

Microstructure of reaction rims

All experiments resulted in polycrystalline dolomite reaction rims with two spatially separated regions of 1) elongated palisades oriented perpendicular to the interface with magnesite and 2) granular equiaxed dolomite grains in contact with calcite. In addition, the pure calcite reactant close to the dolomite rim transformed to polycrystalline magnesio-calcite. The layer width was defined petrographically by the occurrence of new formed grains using an optical microscope. Microprobe analyses confirm these new formed grains to be magnesio-calcite with decreasing magnesium content towards pure calcite (see **Figure 7**). The thickness of the magnesio-calcite layer is about 4 times that of the entire dolomite rim (**Table 2**). The size of the magnesio-calcite grains increases from the dolomite reaction rim towards the pure calcite starting material (

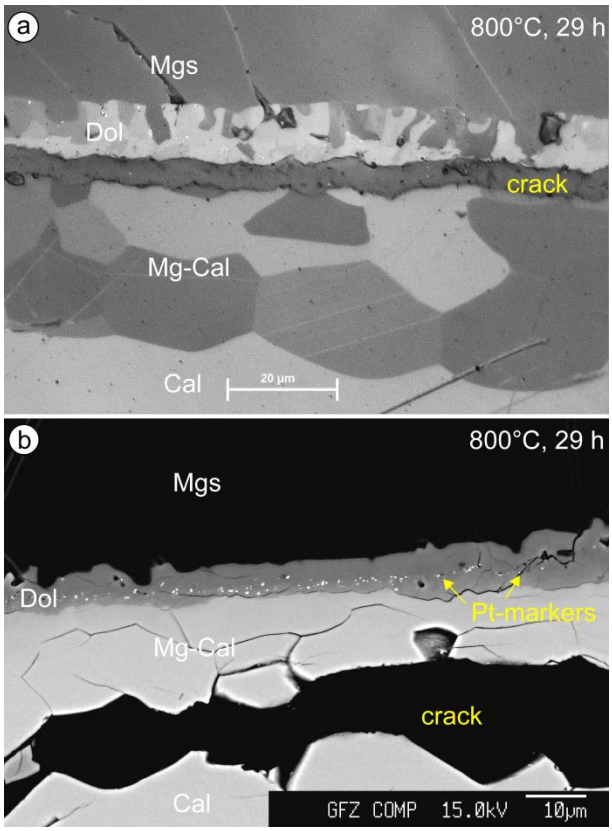

Figure 3 Pt-marker experiment CaMg-14, annealed at 800°C and 29 h run duration. **a** Optical micrograph of polycrystalline dolomite and magnesio-calcite layers between magnesite and calcite single crystals. The dolomite rim consists of palisades oriented perpendicular to the interface with magnesite and of granular dolomite in contact to magnesio-calcite. **b** BSE image showing platinum markers (white spots), which indicate that the original calcite-magnesite interface is located at the boundary between the domains of the palisade-like and granular dolomite. Outliers are attributed to dolomite grain growth during annealing. Open cracks between interfaces are expected to evolve during cooling and sample preparation

a). The grains often show curved grain boundaries with equilibrium angles at triple junctions. The platinum marker experiments indicate that the original interface between the reactants is located between dolomite palisades and granular dolomite (

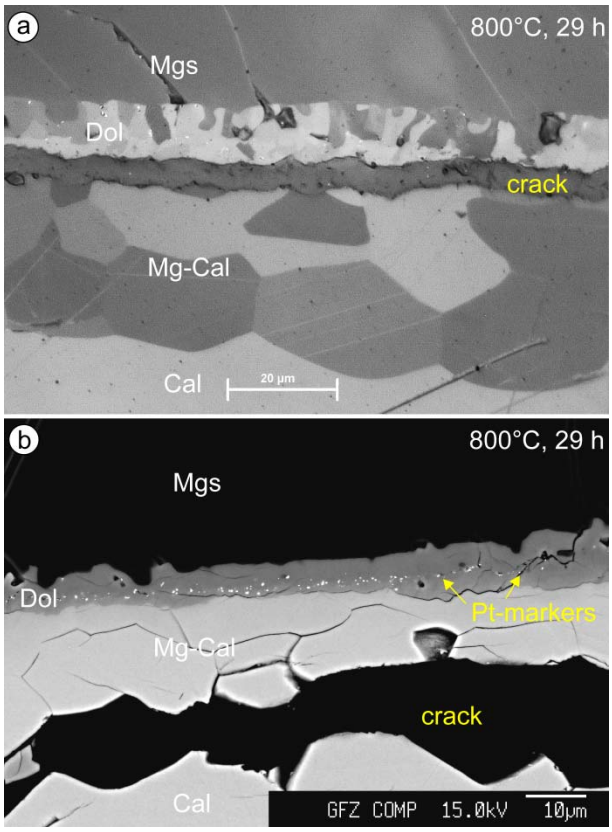

Figure 3 Pt-marker experiment CaMg-14, annealed at 800°C and 29 h run duration. **a** Optical micrograph of polycrystalline dolomite and magnesio-calcite layers between magnesite and calcite single crystals. The dolomite rim consists of palisades oriented perpendicular to the interface with magnesite and of granular dolomite in contact to magnesio-calcite. **b** BSE image showing platinum markers (white spots), which indicate that the original calcite-magnesite interface is located at the boundary between the domains of the palisade-like and granular dolomite. Outliers are attributed to dolomite grain growth during annealing. Open cracks between interfaces are expected to evolve during cooling and sample preparation

b).

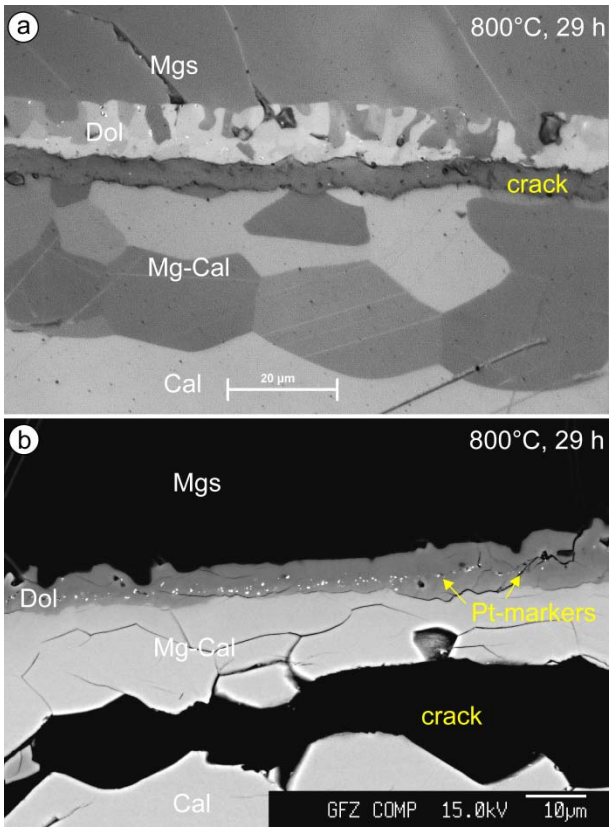

Figure 3 Pt-marker experiment CaMg-14, annealed at 800°C and 29 h run duration. **a** Optical micrograph of polycrystalline dolomite and magnesio-calcite layers between magnesite and calcite single crystals. The dolomite rim consists of palisades oriented perpendicular to the interface with magnesite and of granular dolomite in contact to magnesio-calcite. **b** BSE image showing platinum markers (white spots), which indicate that the original calcite-magnesite interface is located at the boundary between the domains of the palisade-like and granular dolomite. Outliers are attributed to dolomite grain growth during annealing. Open cracks between interfaces are expected to evolve during cooling and sample preparation

Kinetics of reaction rim growth

Time series experiments were done at temperatures of 750 and 800°C by varying the annealing time between 3 and 146 hours. For determining the temperature dependence of the reaction kinetics, the temperature was varied between 750 and 850°C at a fixed time of 74 hours. Generally, we find increasing rim thicknesses and grain sizes with increasing annealing time and temperature (**Table 2**). **Figure 4** shows rim thickness as a function of square root of time for all rim growth experiments. Both time series at temperatures of 750°C and 800°C reveal a linear increase of dolomite rim width with increasing square root of time, following a power law form of $\Delta x^2 = kt$ and consequently indicating diffusion-controlled rim growth (JOESTEN 1977; JOACHIM ET AL. 2010; ABART ET AL. 2009). In comparison, at similar temperature and time the magnesio-calcite layer is thicker than the entire dolomite layer, whereas granular and elongated dolomite rims are approximately equal in width.

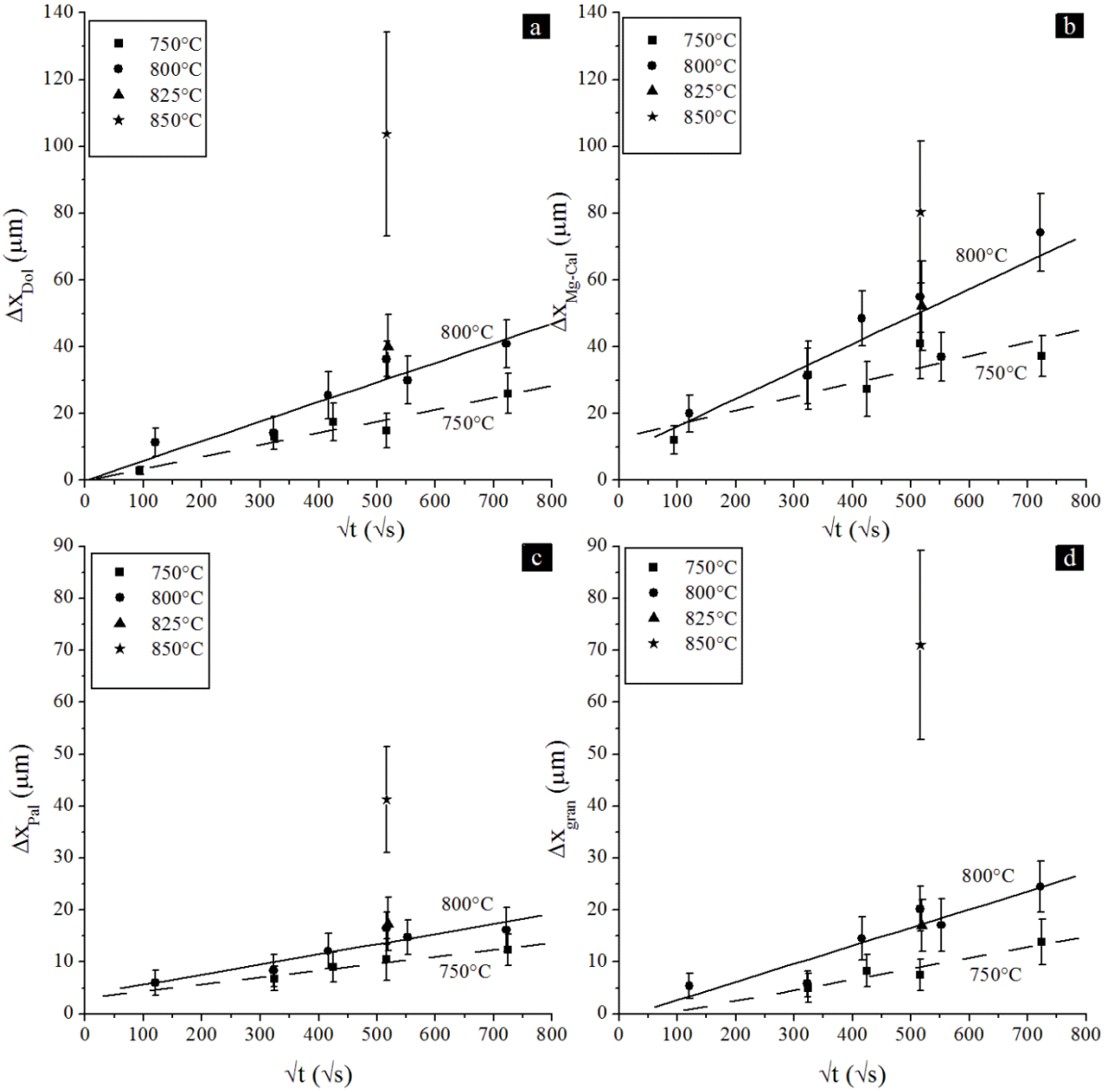

Figure 4 Reaction product layer width versus square root of time, linear relations are indicated for T = 750°C (dashed lines) and 800°C (solid lines). **a** Total dolomite reaction rim width, **b** magnesio-calcite width, **c** dolomite palisades width, and **d** granular dolomite thickness. Error bars reflect the relatively large thickness variation (12-41%) along each profile of 7 mm length. Note different scales

For example, for the time series performed at T = 750°C, the average thickness of dolomite reaction rims varies between 2.9 and 26 µm and that of magnesio-calcite between 12.1 and 40.9 µm, respectively. At 800°C the values range from 11.3 to 40.9 µm for the entire dolomite and 31.2 to 74.2 µm for the magnesio-calcite layer. The thicknesses of magnesio-calcite and dolomite palisades show a fast non-linear incipient stage (**Figure 4 b, c**), while granular dolomite growth is retarded (**Figure 4 d**). Afterwards the layer thicknesses increase linearly with the square root of time following a parabolic growth behavior. Grain coarsening of dolomite palisades, granular dolomite and magnesio-calcite takes place during the experiments. Palisades and granular

dolomite grain sizes increase by a factor of 1.5-1.8 at 750°C and 1.5-1.6 at 800°C during run durations between 29 and 145 hours (**Table 2**). In the same time span, the average magnesio-calcite grains coarsen about a factor of 1.4 and 1.7 (**Table 2**).

The different slopes of the regression lines for T = 750°C and 800°C shown in **Figure 4** indicate that the temperature sensitivity of rim growth is lowest for dolomite palisades and highest for magnesio-calcite. Extending the temperature range to 850°C suggests that at a constant annealing time of 74 h the ratio of $\Delta x_{Dol}/\Delta x_{Mg\text{-}Cal}$ increases with T and exceeds 1 at about 840°C (**Figure 5**). In contrast, the ratio of $\Delta x_{Pal}/\Delta x_{gran}$ decreases with temperature from 1.4 to 0.58 (**Figure 5 b**), suggesting a lower temperature sensitivity for growth of dolomite palisades than of granular dolomite.

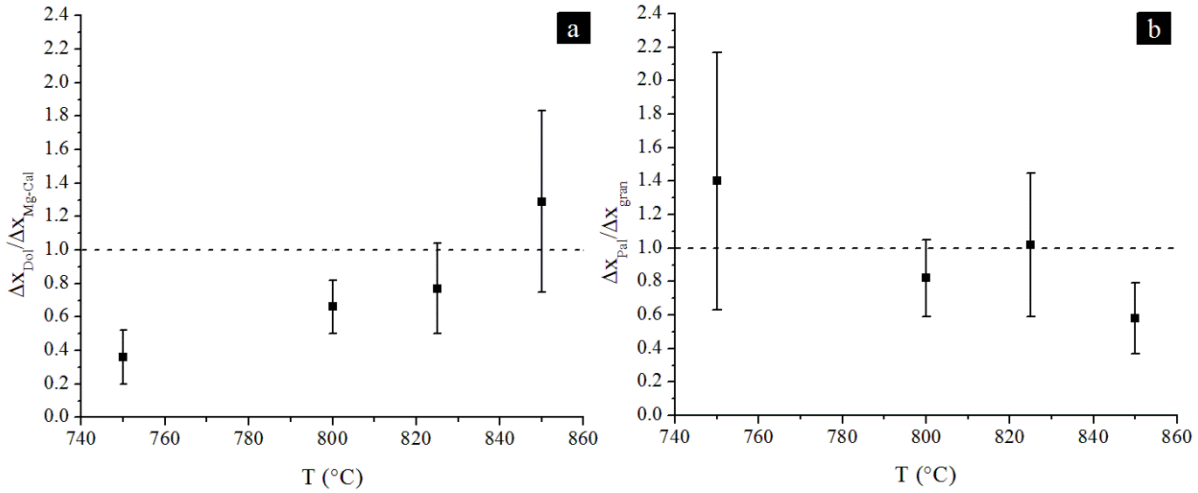

Figure 5 a Dolomite rim/magnesio-calcite thickness ratio versus temperature. The thickness ratio increase with increasing temperature. **b** Dolomite palisades/granular dolomite thickness ratio versus temperature. The thickness ratio tends to decrease with increasing temperature

Texture analyses

Detailed crystallographic orientation maps were measured in 9 selected samples including the orientation of calcite and magnesite single crystals, polycrystalline dolomite (palisade and granular shapes) and polycrystalline magnesio-calcite. A typical orientation map and pole figures are presented in **Figure 6**, using the inverse pole figure color coding (see inset for details). The orientations of calcite and magnesite starting material single crystals are constrained by the orientation of one of the three $\{10\bar{1}4\}$ poles parallel to the growing direction (GD), since one of the three symmetric rhomb planes was parallel to the initial reaction interface (**Figure 6 a**). The resulting bulk texture for dolomite shows [0001] axes for both palisades and granular dolomite concentrated in a position normal to the GD, with secondary concentrations (principally for the palisades) spreading all over the pole figures (**Figure 6 a**). The poles of $\{2\bar{1}\bar{1}0\}$ prismatic planes are distributed in a more complex form with no clear relation between maximum concentrations and external reference frame. The poles of $\{10\bar{1}0\}$ prismatic planes on the other hand form broad girdles normal to the reaction interface with weak maxima parallel to GD. The $\{10\bar{1}4\}$

rhombs are also distributed in a complex way, and the maxima of these poles tend to lie within the reaction interface plane (**Figure 6 a**). In contrast, magnesio-calcite forms [0001] axes subparallel or oblique to GD, poles of $\{2\bar{1}\bar{1}0\}$ and $\{10\bar{1}0\}$ form broad girdles subparallel to the reaction interface, and poles to $\{10\bar{1}4\}$ form small circles around the growing direction axis (**Figure 6 a**). Although the dolomite orientations show considerable scattering, the bulk texture still indicates some crystallographic orientation relationship to magnesite but primarily to calcite single crystals (see labels **1-6** in **Figure 6 a**). Detailed analysis of EBSD data revealed the presence of dolomite growth twins characterized by a rotation of 180° around one of the three equivalent a-axes ($[11\bar{2}0]$ twin axis). The twin grain boundaries represent between 25 and 40 % of dolomite-dolomite boundaries in all the analyzed samples (see black lines decorating the twin boundaries in the EBSD map and histogram of misorientation in **Figure 6 a**). Although the twin grains occur within granular and palisades parts of the dolomite rim, the proportion of twin grains prevails in granular dolomite. Furthermore a topotactic relationship, where all crystallographic directions of dolomite are fixed with respect to the calcite single crystal, could be observed in all samples (e.g. **Figure 6 b**). These topotactic grains often appear equiaxed in shape and are characterized by the above-described twin relationship. Even within the magnesio-calcite layer, grains with the topotactic relationship to the calcite single crystal are present in most analyzed samples (e.g. **Figure 6 b**). The dolomite bulk texture diagrams (**Figure 6 a**) indicate axiotactic (only one crystallographic direction parallel) relationships of dolomite $\{2\bar{1}\bar{1}0\}$ and $\{10\bar{1}0\}$ axes to both calcite and magnesite single crystals (labeled **2, 5** and **6** in **Figure 6 a**). Furthermore, weak axiotactic relationship of rhombohedral crystallographic directions in dolomite to single crystal calcite may be suspected from the dolomite bulk texture diagrams (labeled **3** and **4** in **Figure 6 a**).

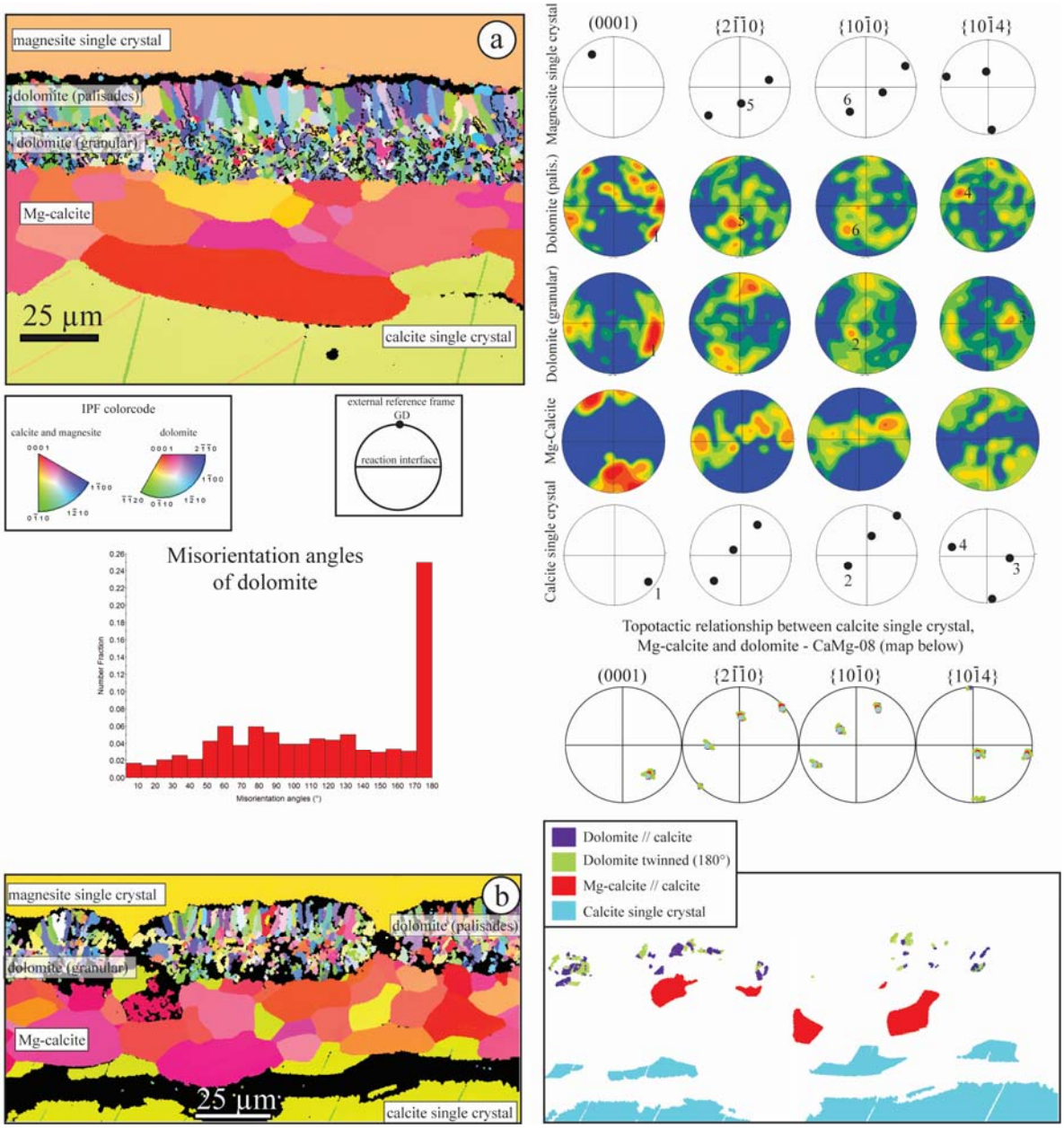

Figure 6 a EBSD inverse pole figure (IPF) color-coded map of sample CaMg-05 (146 h, 750 °C), showing the orientation of magnesite and calcite single crystals, polycrystalline dolomite (palisades and granular shapes) and magnesio-calcite. IPF color-code indicates the orientation of reference axes parallel to the growing direction (GD). For example, red or light blue grains have the $[1\bar{2}10]$ / [0001] or $[1\bar{2}10]$ axis pointing to the reader (note different colors for different phases). Black lines within dolomite rim highlight the twin relationship between neighboring dolomite grains. The histogram below shows the correlated misorientation angles of dolomite indicating that 26 % of all dolomite-dolomite boundaries are represented by twin boundaries. Pole figures for [0001] axes, poles to prismatic $\{2\bar{1}\bar{1}0\}/\{10\bar{1}0\}$ and rhomb $\{10\bar{1}4\}$ planes are plotted with respect to the external reference frame. The reference frame is defined by E-W plane, which represents the reaction rim interface and GD of the rim which is oriented N-S. The numbers on the pole figures indicate individual orientation relationships between calcite single crystal and dolomite (**1-4**) and magnesite and dolomite (**5-6**). All pole figures are equal-area projections (lower hemisphere) with a Gaussian half-width of 10° and a confidence index (CI) >0.2. Contour color densities are drawn based on multiples of random distribution with a factor of 9 from blue to red. **b** EBSD inverse pole figure color-coded map of sample CaMg-08 (48 h, 800 °C), which best documents the topotactic relations to single crystal calcite reactant. The map on the right shows grains of dolomite (dark blue) and magnesio-calcite (red) with topotactic relations to calcite (light blue) demonstrated in the pole figures. The light green grains in the topotaxy map represent the twinned dolomite grains in relation to the dark blue ones that show the topotactic relationships described before

Microprobe analyses

Compositional line scans were performed from one reactant to the other across the dolomite rim and magnesio-calcite layer to measure chemical profiles (**Figure 7**). While the composition of the reactant phases is homogenous and flat also adjacent to the reaction rims, composition gradients occur within the newly evolved magnesio-calcite and dolomite rims. The dolomite is close to stoichiometric at the dolomite-magnesite interface, and it becomes successively more non-stoichiometric with increasing Mg deficiency towards the dolomite-calcite interface. According to the phase diagram in

Figure 2, dolomite in equilibrium with magnesio-calcite at 800°C should have a composition with about 47 mol % $MgCO_3$component and a dolomite in equilibrium with magnesite should have about 51 mol % $MgCO_3$ component. The composition of dolomite at the dolomite-magnesite interface thus closely corresponds to local equilibrium. In contrast, the dolomite is more calcium-rich and the magnesio-calcite is somewhat more Mg-rich than what is expected for local equilibrium at the calcite-dolomite interface. The processes underlying this deviation from local equilibrium are not known. A possible explanation could be the three dimensional character of the microstructures, which would especially influence analyses at phase boundaries, or the effect of nucleation and interface-reaction at the initial stage of rim growth, which appears to be fast for dolomite palisades (**Figure 4 c, d**). Alternatively, the depletion of Mg in granular dolomite due to the preceding magnesio-calcite formation may induce local disequilibrium in granular dolomite. The effect of deviations from local equilibrium element partitioning on the overall reaction kinetics are considered as minor and this complication has not been accounted for in our thermodynamic model. Magnesio-calcite always shows a curved profile with progressively decreasing Mg content from granular dolomite towards calcite. Measurements on 10 samples at different run durations and temperatures reveal two different CaO and MgO distributions in dolomite, illustrated in **Figure 7**. At T = 850°C, the dolomite palisades are nearly stoichiometric. The granular dolomite is substantially more Ca-rich and is clearly non stoichiometric with respect to its Ca/Mg ratio towards the contact with magnesio-calcite (**Figure 7 a**). At T = 825°C, the molar concentrations of CaO and MgO are similar at the initial interface (dashed line in **Figure 7 b**). Chemical profiles of the other samples show the same two trends, but no systematic variation with annealing time or temperature.

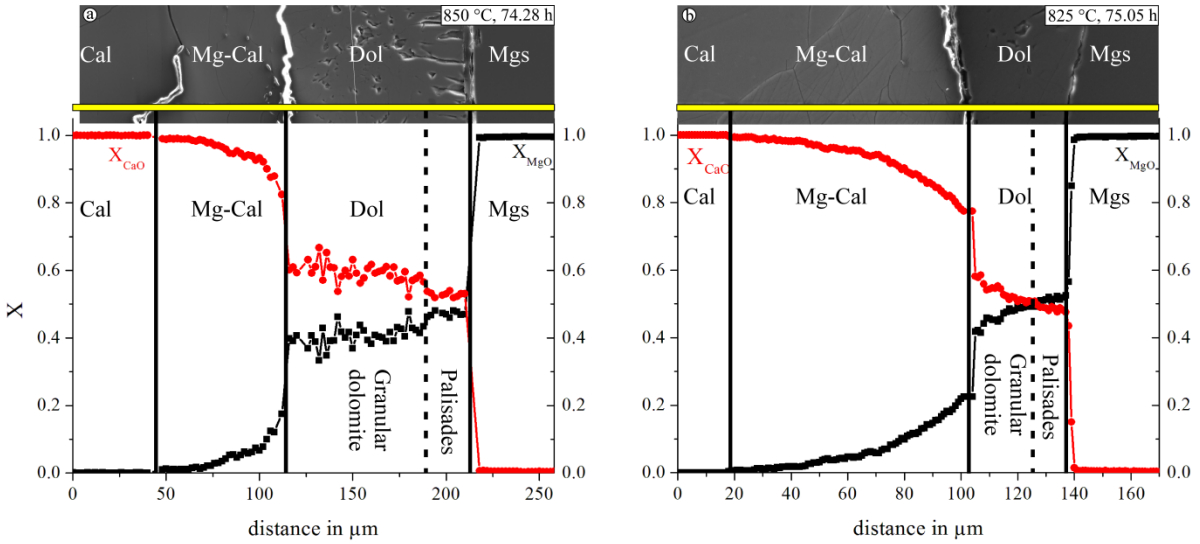

Figure 7 Chemical profiles in **a** sample CaMg-10 (t = 74.28 h, T = 850 °C) and **b** sample CaMg-13 (t = 75.05 h, T = 825°C). The mole fractions of calcium (X_{CaO}) and magnesium (X_{MgO}) are shown in red and black, respectively. Solid vertical lines indicate locations of phase boundaries while the dashed line indicates the original interface

Discussion

Microstructure and texture evolution

Initial reaction phase during experiments is associated with the formation of magnesio-calcite (

Figure 2), which grew towards the calcite single crystal. This initial re-equilibration is assumed to affect the reaction interface, so that dolomite formed in between single crystal magnesite and polycrystalline magnesio-calcite. Such setup is probably responsible for the development of the two distinct dolomite regions. Granular dolomite encountered boundaries of already existing magnesio-calcite grains, while palisades could grow into the magnesite single crystal. The elongated shape of dolomite in contact with magnesite is suggested to be a stress-induced phenomenon resulting from a positive volume change at the dolomite-magnesite reaction interface (MILKE AND WIRTH 2003). Although, the overall reaction is more or less balanced regarding the volume change, the partial reaction at the magnesite-dolomite interface implicates a positive volume change, while the incorporation of magnesium in calcite results in a negative volume change.

Since magnesio-calcite results from magnesium incorporation into calcite, it is likely that magnesio-calcite grains may inherit the crystallographic orientation of pure calcite. Indeed, some of the magnesio-calcite grains show a full crystallographic relation to calcite, which is then transferred also into dolomite (**Figure 6 b**). The relatively large size of the magnesio-calcite grains implies few nucleation sites, possibly because of the small composition contrast across the magnesio-calcite / calcite interface (**Figure 7**). The dolomite grains with topotaxy to calcite reactant occur mainly in the granular part of the rim or near the original reaction interface. They are characterized by a slightly larger grain size than the average and their spatial occurrence usually coincide with slightly thinner rim portions (**Figure 6 b**). This correlation may be

explained by a slightly hindered grain boundary diffusion and nucleation during the initial phases of the rim growth in topotactic domains.

1.1.1 Diffusion components

The parabolic growth behavior of the dolomite reaction rim suggests that diffusion of Mg and/or Ca components was rate limiting (**Figure 4 a**; FISHER 1978). The term component is used here as a mere chemical entity that suffices to describe the chemical variation in the system of interest. It does not necessarily correspond to the composition of a phase or species. Within a single crystal of dolomite mass transfer may occur via interdiffusion of Mg^{2+} and Ca^{2+} ions. In this case, the cation fluxes are forced to be equal and directed in opposite directions due to the charge-balance constraint. Alternatively, Mg^{2+} and Ca^{2+} may diffuse coupled with O^{2-}, which would make Ca- and Mg-fluxes independent. Such behavior is probably enhanced through the presence of lattice imperfections such as edge dislocations and, more importantly, of grain boundaries, which could act as sources and sinks of vacancies. In case of a fine-grained polycrystalline reaction rim the coupled diffusion of divalent cations and oxygen is thus conceivable. Based on experiments in the $MgO\text{-}SiO_2$ system (GARDÉS AND HEINRICH 2011) and in the CaO-$MgO\text{-}SiO_2$ system (Joachim et al. 2010), which were both conducted under "dry" conditions, coupled diffusion of Mg^{2+} and O^{2-} could indeed be demonstrated. During growth of a polycrystalline dolomite reaction rim in the two component system $MgCO_3$ - $CaCO_3$ the diffusion fluxes of the two components may be independent. In our study, we do not consider transfer of carbonate. It is thus sufficient to consider MgO and CaO as the two mobile components. Although the speciation of the diffusing matter is not known, the bulk effect of its transfer can be descried in terms of the MgO and CaO components. If the Mg and the Ca–bearing species indeed diffuse independently, the rim growth rate depends on the mobilities of both components. The relative fluxes of the two components can be inferred from the position of the original calcite-magnesite interface (ABART ET AL. 2004). The off-center position of the original calcite-magnesite interface as indicated by the platinum markers (

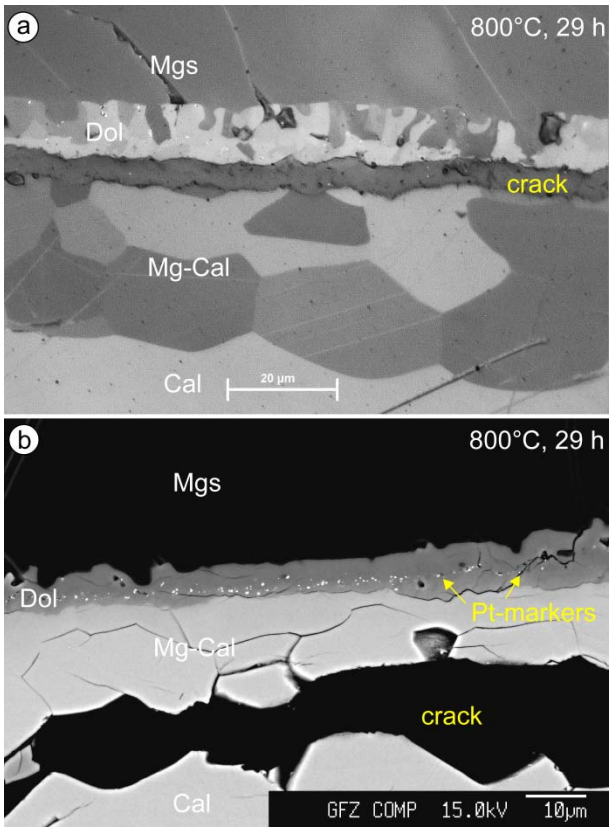

Figure 3 Pt-marker experiment CaMg-14, annealed at 800°C and 29 h run duration. **a** Optical micrograph of polycrystalline dolomite and magnesio-calcite layers between magnesite and calcite single crystals. The dolomite rim consists of palisades oriented perpendicular to the interface with magnesite and of granular dolomite in contact to magnesio-calcite. **b** BSE image showing platinum markers (white spots), which indicate that the original calcite-magnesite interface is located at the boundary between the domains of the palisade-like and granular dolomite. Outliers are attributed to dolomite grain growth during annealing. Open cracks between interfaces are expected to evolve during cooling and sample preparation

), suggests that the diffusive fluxes of the two components were different.

1.1.2 Dolomite rim growth model

The overall reaction (**1**) can be split into two partial reactions, taking place at the dolomite-calcite (**1**) magnesite-dolomite (**2**) and the interface:

$$\text{Interface I:} \quad CaCO_{3,solid} + \nu\, MgCO_{3,mobile} = \nu\, CaMg(CO_3)_{2,solid} + (1-\nu)\, CaCO_{3,mobile} \qquad (\mathbf{1})$$

$$\text{Interface II:} \quad MgCO_{3,solid} + (1-\nu)\, CaCO_{3,mobile} = (1-\nu)\, CaMg(CO_3)_{2,solid} + \nu\, MgCO_{3,mobile} \qquad (\mathbf{2})$$

where ν is the molar amount of MgO forming granular dolomite at the calcite-dolomite interface and (1- ν) is the molar amount of CaO producing dolomite palisades from magnesite at the dolomite-magnesite interface. In

Figure 8 the geometry of the rim growth setting and the associated component fluxes are illustrated schematically.

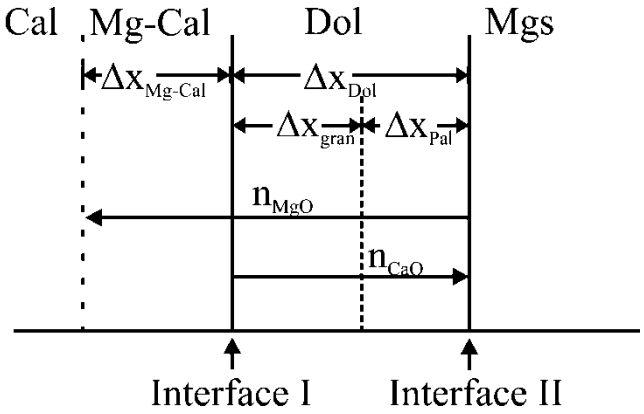

Figure 8 Schematic drawing of the growth of dolomite and magnesio-calcite at a calcite-magnesite contact in planar geometry (adopted from ABART ET AL. 2009). The decomposition of magnesite at interface I provides mobile MgO, and the decomposition of calcite at interface II provides mobile CaO. The dashed line within the dolomite layer represents the boundary between dolomite palisades and granular dolomite, i.e. the position of the initial interface between the reactant phases

Within the dolomite rim the domains with the palisade and the granular microstructures are discerned. Note that the flux of CaO is restricted to the rim of newly formed dolomite; in contrast a fraction of the MgO that is derived from the consumption of the magnesite at the dolomite-magnesite interface diffuses across the dolomite-calcite interface and into the calcite forming magnesio-calcite. The fraction ν is related to the molar amount (n) of components that are transferred during reaction rim growth

$$v = \frac{n_{MgO}}{n_{MgO} + n_{CaO}} \tag{3}$$

where *n* can be derived from the thickness of dolomite layers Δx_{pal} and Δx_{gran}, the molar volume $\bar{V}^{\gamma}$ of phase γ and the unit cross section A.

$$n_{CaO} = \frac{\Delta x_{pal}\, A}{\bar{V} dol} \tag{4}$$

$$n_{MgO} = \frac{\Delta x_{gran}\, A}{\bar{V} dol} + \frac{\Delta x_{Mg-Cal}\, c_T\, A}{\bar{V} Cal} \tag{5}$$

The second term in equation (**5**) accounts for the formation of magnesio-calcite. The correction factor $c_T$represents the molar Mg concentration, which was determined from measured chemical profiles leading to average values of $c_{750,850} = 0.03$, $c_{800} = 0.04$ and $c_{825} = 0.06$ at T = 750°C and 850°C, 800°C and 825°C, respectively.

To determine the diffusion coefficients of CaO and MgO the thermodynamic model for diffusion controlled reaction rim growth in a binary system of ABART ET AL. (2009) with extension of GÖTZE ET AL. (2009) was used. This model is based on the assumption that the diffusion of chemical components across the dolomite reaction rim is the only dissipative process and that the potential contribution of dolomite nucleation to the total energy budget can be neglected. Rearrangement of equations 26, 34 and 36 from ABART ET AL. (2009) leads to the combined diffusion coefficient (D_{com}) which accounts for the simultaneous diffusion of both mobile components MgO and CaO:

$$D_{com} = R_g T \frac{\Delta x_{pal}^2 (1-u)}{2t\Delta G_{rim}} \frac{\left(X_{MgO}^{Mgs} X_{CaO}^{Dol} - X_{MgO}^{Dol} X_{CaO}^{Mgs}\right)^2}{(v-1)X_{MgO}^{Dol} - vX_{CaO}^{Dol}} \frac{V^{Dol}}{(V^{Mgs})^2} \frac{1}{X_{CaO}^{Dol} X_{MgO}^{Dol}} \quad (6)$$

where R_g is the gas constant, V^{γ} is the specific molar volume of phase γ, and X_i^{γ} is the mole fraction of component i in phase γ. The parameter u incorporates the mass balance at the reaction fronts and information of interface motions (ABART ET AL. 2009). Since the original model assumes stoichiometric composition of the reaction rim, we account for the measured chemical gradient in dolomite

Figure 8 by using a modified expression for u using equations 14,15,17,18 and 21 of Abart et al. (2009), which leads to (GÖTZE ET AL. 2009):

$$u = 1 - \frac{V^{Dol}}{V^{Mag}} \left[\frac{v(1-2X_{CaO}^{Mgs}) - (1-X_{CaO}^{Mgs})}{v(1-2X_{CaO}^{Pal}) - (1-X_{CaO}^{Pal})} - \frac{\frac{-v(1-2X_{CaO}^{Cal}) + (1-X_{CaO}^{Cal})}{X_{CaO}^{Cal} X_{MgO}^{gran} - X_{MgO}^{Cal} X_{CaO}^{gran}}}{\frac{-v(1-2X_{CaO}^{Pal}) + (1-X_{CaO}^{Pal})}{X_{CaO}^{Mgs} X_{MgO}^{Pal} - X_{MgO}^{Mgs} X_{CaO}^{Pal}}} \right] \quad (7)$$

The mean mole fractions at the reaction fronts for a given temperature were determined from microprobe analysis. The Gibbs molar energy of rim formation (ΔG_{rim}) is defined by the ratio of the molar Gibbs free energy of the reaction ($\Delta_r G$) to the specific molar volume of magnesite (V^{Mgs}) (ABART ET AL. 2009; their equation 27):

$$\Delta G_{rim} = \frac{1}{V^{Mgs}} \Delta_r G \quad (8)$$

The thermodynamic data of the phases in our experiments used to calculate ΔG_{rim} are given in Table 3. The combined diffusion coefficient D_{com} can also be expressed by (ABART ET AL. 2009):

$$D_{com} = kD_{MgO} + (1-k)D_{CaO}, \quad (9)$$

where k gives the proportion of the component fluxes within the dolomite reaction rim defined as

$$k = \frac{D_{MgO}}{D_{MgO} + D_{CaO}} \quad (10)$$

Combining equations (**9**) and (**10**) allows determining the individual component diffusivities:

$$D_{CaO} = D_{com} \frac{(1-k)}{(2k^2-2k+1)} \quad \text{and} \quad D_{MgO} = \frac{D_{com} - D_{CaO}(1-k)}{k} \quad (11)$$

The diffusion coefficients obtained from our rim growth experiments are shown in an Arrhenius diagram in **Figure 9**, following the relation:

$$D = k_0 e^{-\frac{E_a}{TR_g}} \quad (12)$$

with k_0 (CaO) = $10^{-4.9 \pm 2.7}$ m²/s, E_a (CaO) = 192 ± 44 kJ/mol and k_0 (MgO) = $10^{-4.5 \pm 2.2}$ m²/s, E_a (MgO) = 198 ± 54 kJ/mol respectively.

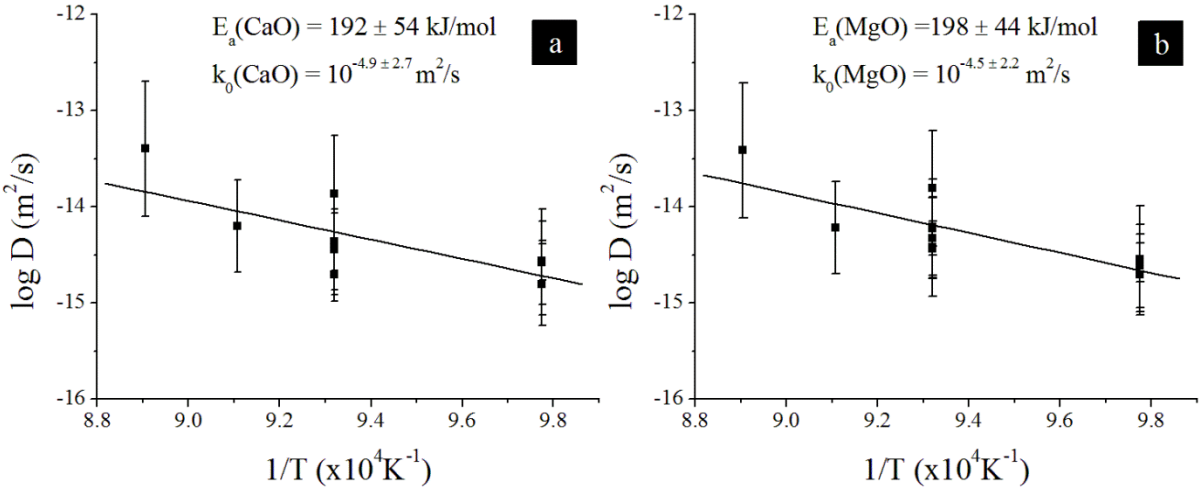

Figure 9 Arrhenius plot of the effective diffusion coefficients of **a** CaO and **b** MgO in dolomite in the range of 750-850°C. Values are from **Table 2**

Both components show almost identical temperature dependence of their diffusivities, which yields quite similar activation energies in the order of 200 kJ/mol for both components. Out of **Figure 5**, a huge difference in activation energies may have been expected due to the increasing or decreasing ratio of layer thicknesses with temperature. Indeed, if plotting the ratio of $\Delta x_{Pal}/(\Delta x_{gran} + \Delta x_{Mg\text{-}Cal})$ against time the ratio remains nearly constant between 0.22 – 0.27, implying similar activation energies for diffusing components.

It must be noted, that the diffusion coefficients refer to the self-diffusion of CaO and MgO in polycrystalline dolomite, where diffusion may occur by a combination of volume- and grain-boundary diffusion. Diffusion coefficients obtained in this study should be regarded as effective diffusion coefficients. The relatively large size of magnesio-calcite grains compared to dolomite grains with magnesio-calcite grain boundaries oriented mainly perpendicular to the growth direction, and the measured chemical profile within magnesio-calcite may indicate dominantly volume diffusion. In contrast, abundant grain boundaries within the small granular dolomite with abundant twins and relatively straight grain boundaries of the dolomite palisades may suggest preferred grain boundary diffusion.

	Calcite	Magnesite	Dolomite
$\bar{V}$ (750°C) [cm³/mol]	37.56	28.72	65.84
$\bar{V}$ (800°C) [cm³/mol]	37.63	28.79	65.98
$\bar{V}$ (825°C) [cm³/mol]	37.67	28.82	66.05
$\bar{V}$ (850°C) [cm³/mol]	37.79	28.85	66.13
$\Delta_f G$ (750°C) [J/mol]	-1,235,207	-1,114,861	-2,354,678
$\Delta_f G$ (800°C) [J/mol]	-1,246,520	-1,124,567	-2,375,712
$\Delta_f G$ (825°C) [J/mol]	-1,252,291	-1,129,530	-2,386,457

$\Delta_f G$ (850°C) [J/mol]	-1,258,138	-1,134,565	-2,397,349

Table 3 Molar volumes $\bar{V}$ and Gibbs free energies $\Delta_f G$ of formation of calcite, magnesite and dolomite at T = 750°C - 850°C and P = 400 MPa (from HOLLAND AND POWELL 1998)

Comparison with other diffusion coefficients in carbonates

To the best of our knowledge only two studies determined component diffusion in dolomite so far. ANDERSON (1972) determined the self-diffusion coefficients of C and O in crushed dolomite using isotope exchange with CO_2 at T = 645-785°C and P = 12-93.5 MPa. Diffusion rates of C and O in dolomite are nearly identical with activation energies of E_a (C) = 468 kJ/mol and E_a (O) = 485 kJ/mol (**Figure 10**).

MÜLLER, CHERNIAK, AND WATSON (2012) performed thin film experiments between dolomite and siderite or rhodochrosite to determine interdiffusion coefficients of (Mn, Fe) – Mg – Ca in the temperature range of 400-625°C at 1 atm pressure. The authors determined coupled diffusion of Mn-(Ca+Mg) d Fe-(Ca+Mg) with activation energies of E_a (Mn-(Ca+Mg)) = 63 ± 5 kJ/mol and E_a (Fe-(Ca+Mg)) = 123 ± 10 kJ/mol respectively. The temperature dependence of the quasi-binary exchange of Mn-Mg and Fe-Mg shows a kink at T ~525°C with an increase of activation energies from E_a (Mn-Mg) = 23 ± 4 kJ/mol to 168 ± 15 kJ/mol and from E_a (Fe-Mg) = 34 ± 10 kJ/mol to 183 ± 14 kJ/mol (**Figure 10**) in a low-temperature regime. A proposed explanation is an increased disorder of dolomite at high temperatures, rather than a transition from an extrinsic to an intrinsic diffusion regime (MÜLLER, CHERNIAK, AND WATSON 2012). When extrapolated to the temperatures of our experiments, the interdiffusion coefficients in the Ca, Mg and Ca, Mg, Mn, Fe-couples determined by MÜLLER, CHERNIAK, AND WATSON (2012) are several orders of magnitude lower than the diffusion coefficients we determined for the CaO and MgO components.

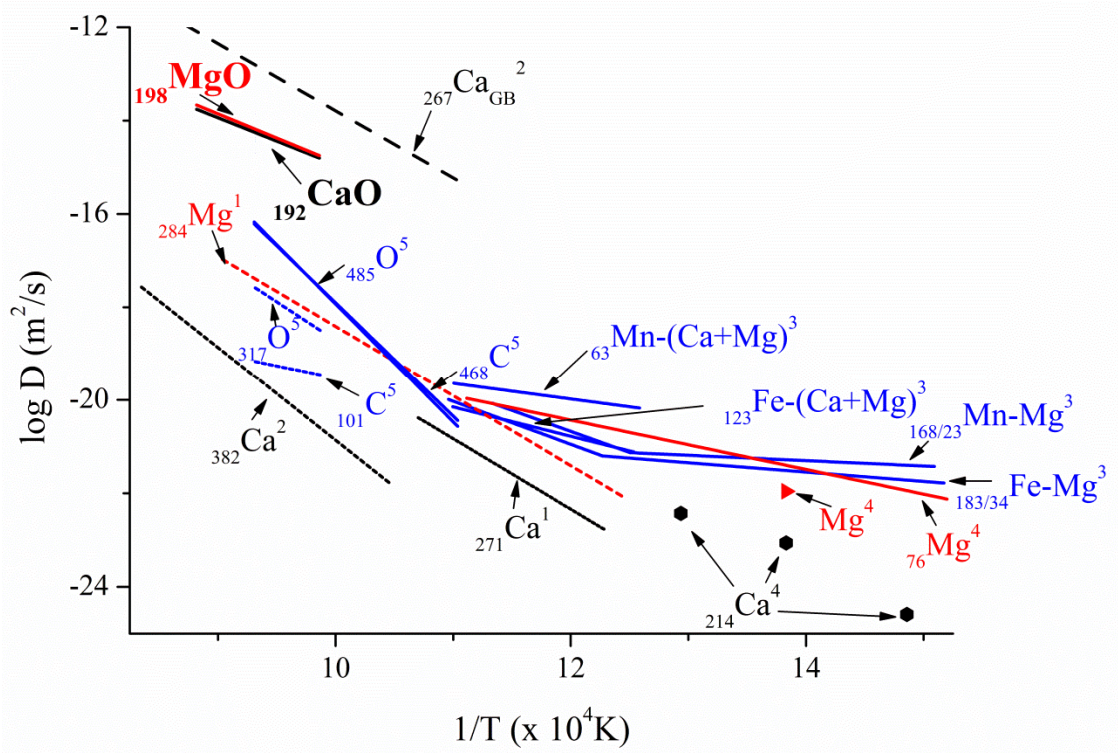

Figure 10 Arrhenius diagram for diffusion coefficients of various elements in calcite, magnesite and dolomite. Published data on diffusion in dolomite and calcite are plotted as solid lines and dashed lines, respectively. Dots and triangles represent chemical diffusion of Ca and Mg in magnesite, respectively. 1 = FISLER AND CYGAN (1999), 2 = FARVER AND YUND (1996), 3 = MÜLLER, CHERNIAK, AND WATSON (2012), 4 = KENT ET AL. (2001), 5 = ANDERSON (1972). Indices at the lower left of the chemical symbols represent activation energies in kJ/mol. All data are determined for volume diffusion, except those marked by GB, which represents grain boundary diffusion

For comparison **Figure 10** also shows diffusion coefficients of Ca and Mg in calcite and magnesite. FARVER AND YUND (1996) determined activation energies for Ca volume and grain boundary diffusion in natural samples at P = 0.1 MPa and T = 650-900°C of 382 ± 37 kJ/mol and 267 ± 47 kJ/mol, respectively. Assuming an effective grain boundary width of 3 nm, diffusion rates would be 6 orders of magnitude higher for diffusion along the grain boundaries than for volume diffusion. Besides, they conducted calcium self-diffusion experiments parallel to the c-axis and perpendicular to the natural cleavage planes of natural calcite single crystals to investigate the anisotropy of diffusion coefficients. Despite the trigonal crystal system there was no anisotropy measureable regarding Ca diffusion in calcite.

FISLER AND CYGAN (1999) measured Ca and Mg self-diffusion coefficients perpendicular to the rhomb plane in natural calcite single crystals. Experiments were performed at T = 550-800°C and P = 0.1 MPa, for which activation energies were quite similar with E_a(Ca) = 271 ± 80 kJ/mol and E_a(Mg) = 284 ± 74 kJ/mol, although Mg self-diffusion appears to be one order of magnitude faster than Ca self-diffusion. Interestingly, the Ca-diffusivity measured by Fisler and Cygan (1999) is one order of magnitude faster than measured by FARVER AND YUND (1996), which may be related to different amounts of Mg and Mn present in the used starting materials (FISLER AND CYGAN, 1999). KENT ET AL. (2001) investigated Mg chemical diffusion in calcite as well as Ca chemical diffusion and Mg self-diffusion in magnesite. Experiments were performed

using fragments of natural cleaved material, calcite or magnesite, which were placed together with dried powder of MgO and $MgCO_3$ for calcite or $CaCO_3$ for magnesite into Pt-capsules. The material was pre-dried and subsequently sealed inside evacuated silica glass tubes for annealing experiments using a muffle furnace. Annealing conditions were between 400 and 600°C at P = 0.1 MPa. For Mg chemical diffusion in calcite an activation energy of only E_a (Mg) = 76 ± 16 kJ/mol was determined, which may indicate a switch from intrinsic to extrinsic diffusion at low T. Chemical diffusion of Ca in magnesite yielded an activation energy of E_a(Ca) = 214 ± 60 kJ/mol. The measured self-diffusion coefficient of Mg in magnesite at 450°C is similar to Mg chemical diffusion in calcite.

These values are higher than those obtained for diffusion of CaO and MgO in our study (E_a (CaO) =192 ± 54 kJ/mol, E_a (MgO) = 198 ± 44 kJ/mol), but overlap within error bars at least for MgO. The associated diffusivities for calcium, magnesium and oxygen volume diffusion in calcite are 3 to 5 orders of magnitude lower than those estimated for dolomite (**Figure 10**).

FARVER AND YUND (1996) measured also the grain boundary diffusion of calcium in natural and hot-pressed calcite aggregates, yielding an activation energy of $E_{a,GB}$(Ca) = 267 ± 47 kJ/mol. Assuming a grain boundary width of 1 nm, FARVER AND YUND (1996) obtained a Ca grain-boundary diffusivity in calcite that is about two orders of magnitude faster than the component diffusivities in dolomite measured in our study (**Figure 10**). Although differences in the calculated diffusivities may arise from the applied experimental techniques, comparison of all of these diffusion data does not clearly demonstrate whether volume or grain boundary predominates in our dolomite rim growth experiments.

Conclusions

Annealing experiments on calcite and magnesite single crystals produced a magnesio-calcite layer and a polycrystalline dolomite reaction rim at temperatures between 750 and 850 °C and 400 MPa confining pressure. Within dolomite, two different microstructural domains formed. Stress-induced palisades grew perpendicular to the interface on magnesite and granular dolomite formed on magnesio-calcite. Platinum markers showed that this microstructural boundary represents the original calcite-magnesite interface. Chemical composition of palisades is nearly stoichiometric, while the granular portions show a slight gradient diverging toward magnesio-calcite. All reaction domains, magnesio-calcite, palisades and granular dolomite show a crystallographic orientation relationship to the calcite reactant. Full crystallographic relationships with respect to calcite are restricted to magnesio-calcite and granular dolomite. Axiotactic dolomite grains also appear in the palisade domain, associated with randomly distributed growth twins. The entire dolomite rim thickness increases linearly with the square root of time, indicating a diffusion-controlled mass transport. Thermodynamic considerations lead to activation energies of E_a (CaO) =192 ± 54 kJ/mol and E_a (MgO) = 198 ± 44 kJ/mol.

Acknowledgments We are grateful to S. Gehrmann for sample preparation, M. Naumann for technical support with the Paterson apparatus and W. Heinrich for fruitful discussions. Two anonymous reviewers are thanked for their insightful comments. This work was funded by the Deutsche Forschungsgemeinschaft within the framework of FOR 741, project RY 103/1-1, which is gratefully acknowledged.

References

Abart R, Schmid R, Harlov D (2004) Silicon and oxygen self-diffusion in enstatite polycrystals: the Milke et al. (2001) rim growth experiment revisited. Contrib Mineral Petrol 147:633-646, doi: 10.1007/s00410-004-0596-9

Abart R, Petrishcheva E, Fischer FG, Svoboda J (2009) Thermodynamic model for diffusion controlled reaction rim growth in a binary system: application to the forsterite-enstatite-quartz system. Am J Sci 309:114-131, doi: 10.2475/02.2009.02

Abart R, Petrishcheva E (2011) Thermodynamic model for reaction rim growth: interface reaction and diffusion control. Am J Sci 311:517-527, doi:10.2138/am.2011.3820

Adams BL, Wright SI, Kunze K (1993) Orientation imaging: The emergence of a new microscopy. Met Trans 24A:819–831, doi: 10.1007/BF02656503

Anderson TF (1972) Self-Diffusion of Carbon and Oxygen in Dolomite. J Geophys Res 77:857-861, doi: 10.1029/JB077i005p00857

Ashworth JR, Sheplev VS, Bryxina NA, Kolobov VY, Reverdatto VV (1998) Diffusion controlled corona reaction and overstepping of equilibrium in a garnet granulite, Yenisey Ridge, Siberia. J Metam Geol 16:231-246, doi: 10.111/j.1525-1314.1998.00134.x

Dohmen R, Milke R (2010) Diffusion in Polycrystalline Materials: Grain Boundaries, Mathematical Models, and Experimental Data. Rev Mineral Geochem 72:921-970, doi: 10.2138/rmg.2010.72.21

Farver J, Yund R (1996) Volume and grain boundary diffusion of calcium in natural and hot-pressed calcite aggregates. Contrib Mineral Petrol 123:77-91

Fisher GW (1978) Rate laws in metamorphism. Geochim Cosmochim Acta 42:1035-1050, doi: 10.1016/0016-7037(78)90292-2

Fisler DK, Cygan RT (1999) Diffusion of Ca and Mg in calcite. Am Mineral 84:1392-1399

Gardés E, Wunder B, Wirth R, Heinrich W (2011a) Growth of multilayered polycrystalline reaction rims in the MgO-SiO_2 system, part I: experiments. Contrib Mineral Petrol 161:1-12, doi:10.1007/s00410-010-0517-z

Gardés E, Heinrich W (2011b) Growth of multilayered polycristalline reaction rims in the MgO-SiO2 system, part II: modelling. Contrib Mineral Petrol 162:37-49, doi:10.1007/s00410-010-0581-4

Gardés E, Wunder B, Marquard K, and Heinrich W, (2012) The effect of water on intergranular mass transport: New insights from diffusion-controlled reaction rims in the MgO-SiO_2 system. Contrib Mineral Petrol 164:1-16, doi:10.1007/s00410-012-0721-0

Goldsmith JR, Heard HC (1961) Subsolidus phase relations in the system $CaCO_3$-$MgCO_3$. J Geol 69:45-74

Gottschalk M, Metz P (1992) The system calcite-dolomite: a model to calculate the Gibbs free energy of mixing on the basis of existing experimental data. N Jb Min Abh 164:29–55

Götze LC, Abart R, Rybacki E, Keller LM, Petrishcheva E, Dresen, G (2010) Reaction rim growth in the System MgO-Al_2O_3-SiO_2 under uniaxial stress. Miner Petrol, 99:263–277, doi:10.1007/s00710-009-0080-3

Holland TJB, Powell R (1998) An internally consistent thermodynamic dataset for phases of petrologic interest. J Met Geol 16:309–343

Joachim B, Gardés E, Abart R, Heinrich W (2011) Experimental growth of åkermanite reaction rims between wollastonite and monticellite: evidence for volume diffusion control. Contrib Mineral Petrol 161:389- 99, doi: 10.1007/s00410-010-0538-7

Joesten R (1977) Evolution of mineral assemblage zoning in diffusion metasomatism. Geochim Cosmochim Acta 41:649-670, doi: 10.1016/0016-7037(77)90303-9

Keller LM, Abart R, Wirth R, Schmid DW, Kunze K (2006) Enhanced mass transfer through short circuit diffusion: Growth of garnet reaction rims at eclogite facies conditions. Am Mineral 91:1024-1038, doi: 10.2138/am2006.2068

Keller LM, Wirth R, Rhede D, Kunze K, Abart R (2008a) Asymmetrically zoned reaction rims: assessment of grain boundary diffusivities and growth rates related to natural diffusion-controlled mineral reactions. J metamorphic Geol 26:99-120, doi:10.1111/j.1525-1314.2007.00747.x

Keller LM, Wunder B, Rhede D, Wirth R (2008b) Component mobility at 900 °C and 18 kbar from experimentally grown coronas in a natural gabbro. Geochim Cosmochim Acta 72:4307-4322, doi: 10.1016/j.gca.2008.05.054

Keller LM, Götze LC, Rybacki E, Dresen G, Abart R (2010) Enhancement of solid-state reaction rates by non-hydrostatic stress effects on polycrystalline diffusion kinetics. Am Mineral 95:1399-1407, doi: 10.2138/am.2010.3372

Kent AJR, Hutcheon ID, Ryerson FJ, Phinney DL (2001) The temperature of formation of carbonate in Martian meteorite ALH84001: constraints from cation diffusion. Geochim Cosmochim Acta 65:311-321, doi: 10.1016/S0016-7037(00)00528-7

Lasaga AC (1983) Geospeedometry: an extension of geothermometry. In: Saxena SK (Ed.) Kinetics and Equilibrium in Mineral Reactions, Springer, New York, 81-114

Milke R, Wiedenbeck M, Heinrich W (2001) Grain boundary diffusion of Si, Mg, and O in enstatite reaction rims: a SIMS study using isotopically doped reactants. Contrib Mineral Petrol 142:15-26, doi: 10.1007/s004100100277

Milke R, Heinrich W (2002) Diffusion-controlled growth of wollastonite rims between quartz and calcite: comparison between nature and experiment. J Metamorph Geol 20:467–480, doi: 10.1007/s00269-003-0304-8

Milke R, Wirth R (2003) The formation of columnar fiber texture in wollastonite rims by induced stress and implications for diffusion-controlled corona growth. Phys Chem Minerals 30:230-242, doi: 10.1007/s00269-003-0304-8

Milke R, Abart R, Kunze K, Koch-Müller M, Schmid D, Ulmer P (2009) Matrix rheology effects on reaction rim growth I: evidence from orthopyroxene rim growth experiments, J. Metamorphic Geol., 27: 71-82, doi: 10.111/j.1525-1314.2008.00804.x

Milke R, Neusser G, Kolzer K, Wunder B (2013) Very little water is necessary to make a dry solid silicate system wet. Geol., 41, 247-250, doi:10.1130/G33674.1

Müller T, Cherniak D, Watson B (2012) Interdiffusion of divalent cations in carbonates: Experimental measurements and implications for timescales of equilibration and retention of compositional signatures. Geochim Cosmochim Acta 84:90-103, doi: 10.1016/j.gca.2012.01.011

Mrowec S (1980) Defects and diffusion in solids: an introduction. Elsevier, Amsterdem

Paterson MS (1970) A high-pressure temperature apparatus for rock deformation. Int J Rock Mech Min Sci 7:517-526, doi: 10.1016/0148-9062(70)90004-5

Schmalzried H (1978) Reactivity and Point Defects of Double Oxides With Emphasis on Simple Silicates. Phys Chem Minerals 2:279-294, doi: 10.1007/BF00308179

Watson EB, Price J (2002) Kinetics of the reaction MgO + Al_2O_3 □ $MgAl_2O_4$ and Al-Mg interdiffusion in spinel at 1200 to 2000°C and 1.0 to 4.0 GPa. Geochim Cosmochim Acta 66:2123-2138, doi: 10.1016/s0016-7037(02)00827-x